SPATIAL MODES AND HELICAL STRUCTURE OF SWIRLING FLOW IN A CYLINDRICAL RESERVOIR WITH A STATIONARY CENTRAL ROD

Milyute E.
Department of Mathematical Computer Science,
Vilnius University and IRG"LITAVEM-3"
Milyus A.
IRG "LITAVEM-3"
Vilnius, Lithuania
https://doi.org/10.5281/zenodo.20186445

Abstract

This work investigates the spatial structure of swirling fluid flow in a cylindrical reservoir with a rotating disk and a stationary central rod. It is shown that an annular shear layer is formed near the rod surface and loses axial symmetry when the local Reynolds number exceeds a critical value. Spectral analysis demonstrates that the observed four-sector structure arises as a result of nonlinear interaction between the dipole mode $m = 2$ and its second harmonic $m = 4$. As the swirl intensity increases, the azimuthal modes acquire a longitudinal phase shift and form a spatial helical shell around the stationary rod. The mechanisms governing the stability of the structure, passive scalar transport, and the formation of secondary recirculation zones are analyzed. It is shown that the resulting structure does not represent an independent concentrated vortex core, but rather a spatially modulated surface of angular momentum transport and vorticity localization. A physical and mathematical model describing the spatial organization of helical modes in swirling flows is proposed.

Keywords: swirling flow; rotating disk; annular shear layer; helical mode; quadrupole instability; non-axisymmetric flow; coherent vortex structures; angular momentum transport; recirculation zones; helical vortex shell; vortex dynamics; cylindrical reservoir; stationary central rod; secondary toroidal vortices; modal instability.

1. Introduction. Swirling flows in confined cylindrical volumes are of considerable interest in fluid dynamics because such structures arise in vortex devices, rotary reactors, turbomachinery, vortex chambers, centrifugal separators, and intensive mixing systems. Particular attention is devoted to flows generated by rotating disks, in which radial momentum transport, axial circulation, and angular momentum redistribution occur simultaneously.

Classical studies of rotating flows demonstrate that, with increasing Reynolds number, an axisymmetric flow structure gradually loses stability and transitions to spatially nonuniform states [1-21]. The best-known examples include Taylor–Couette vortices, vortex breakdown, precessing vortex cores, and azimuthal modal structures.

Studies of swirling flows carried out by Alekseenko, Kuibin, and Okulov [13] are mainly devoted to concentrated vortex cores, helical vortex filaments, coherent structures, and spatial instabilities in swirling flows. These works provide a detailed analysis of the mechanisms responsible for the formation of spiral vortex structures, angular momentum redistribution, and the stability of vortex systems in confined volumes. Particular attention is paid to the spatial organization of vorticity and to the interaction between swirl and internal shear layers.

At the same time, the configuration considered in the present work differs substantially from classical models of concentrated helical vortices. The presence of a stationary central rod prevents the formation of a continuous vortex core in the axial region of the reservoir. As a result, the swirling flow reorganizes into an annular shear layer: $r_s < r < r_s + \delta_s$, where r_s is the radius of the stationary rod and δ_s is the characteristic thickness of the annular shear layer. Within this region, an intense radial gradient of the azimuthal velocity, $\partial u_\varphi / \partial r \neq 0$, is formed and becomes the source of azimuthal instability. When the local Reynolds number $Re_s = U_\varphi \delta_s / \nu$, reaches critical values, where U_φ is the characteristic azimuthal velocity within the annular layer and ν is the kinematic viscosity of the fluid, a non-axisymmetric modal state develops, involving the dipole mode $m = 2$ and its nonlinear harmonic $m = 4$. This mode corresponds to the loss of complete axial symmetry and to the formation of four stable convective regions around the stationary rod. The perturbation field may be represented as

$$u'(r, \varphi, z) = A(r, z) \cos(4\varphi - kz) \quad (1)$$

where $A(r, z)$ describes the spatial distribution of the mode amplitude and k is the longitudinal wavenumber of the helical structure. With further development of the swirl, the quadrupole mode acquires a spatial phase shift along the height of the reservoir, causing the transverse modal structures to merge into a unified three-dimensional helical shell surrounding the stationary rod. Unlike classical helical vortex filaments, the structure considered here does not represent an isolated concentrated vortex core but rather a spatially deformed annular layer of angular momentum transport.

An additional feature of the flow is the vertical transformation of the quadrupole mode. In the lower part of the reservoir, near the rotating disk, the shell possesses high energy and significant inertial stresses,

$$\sigma_i \sim \rho (u_s^2 / R_c), \quad (2)$$

where u_s is the fluid velocity along the helical streamline and R_c is the local radius of curvature of the spatial shell. In this region, the maximum concentration of vorticity, strong nonlinear deformation of the mode, and intense pressure redistribution are observed.

As the distance from the rotating disk increases and the flow moves upward through the reservoir, the amplitude of the spatial deformation decreases because of viscous dissipation and angular momentum redistribution. As a result, the helical shell gradually relaxes, becomes smoother, and approaches a quasi-stationary spatial state. Thus, the considered structure may be interpreted as a nonlinear coherent mode of an annular swirling layer in a confined cylindrical volume containing an internal stationary obstacle.

2. Geometry of the Problem. In the considered problem, a crucial role is played by the stationary central rod, which prevents the formation of a continuous vortex core in the axial region of the reservoir. As a consequence, the swirling flow reorganizes into an annular vortex structure surrounding the internal obstacle, within which an intense azimuthal velocity shear is formed.

The flow regime under consideration corresponds to tangential fluid injection through a side inlet, while a rotating disk transfers angular momentum to the flow. The central rod remains stationary, and the fluid is discharged through the lower part of the reservoir. Under these conditions, a stationary quadrupole azimuthal mode $m = 4$ develops within the annular shear layer, which subsequently transforms into a spatial helical shell as the swirl intensity increases. The investigated system consists of a cylindrical reservoir of radius R and height H. A rotating disk of radius b, rotating with a constant angular velocity Ω is located at the bottom of the reservoir. Along the axis of the reservoir, a stationary central rod of radius r_s is installed. Fluid is supplied tangentially through a side inlet and removed through a lower outlet channel.

The flow is described in cylindrical coordinates (r, φ, z) , where r is the radial coordinate, φ is the azimuthal angle, and, z is the vertical coordinate. The velocity field is represented as

$$\mathbf{u} = u_r \mathbf{e}_r + u_\varphi \mathbf{e}_\varphi + u_z \mathbf{e}_z \,. \quad (3)$$

On the surface of the rotating disk, the rotational boundary condition is imposed: $u_\varphi(r, z = 0) = \Omega r$, where Ω is the angular velocity of the disk. On the surface of the stationary rod, the no-slip condition $u_\varphi(r_s) = 0$ is satisfied, leading to the formation of an intense radial gradient of the azimuthal velocity near the internal obstacle. The no-slip condition is also imposed at the outer wall of the reservoir $u_\varphi(R) = 0$.

Thus, the flow develops within a confined annular region between the stationary rod and the outer wall of the reservoir, where the interaction between rotational motion, viscosity, and geometric confinement gives rise to spatially nonuniform modal structures.

3. Governing Equations. The flow is described by the Navier–Stokes equations for an incompressible fluid:

$$\nabla \cdot \mathbf{u} = 0 \,,$$
$$\rho\big((\partial \mathbf{u}/\partial\, t) + (\mathbf{u} \cdot \nabla)\mathbf{u}\big) = -\nabla p + \mu \nabla^2 \mathbf{u} \,, \quad (4)$$

where $\mathbf{u} = u_r \mathbf{e}_r + u_\varphi \mathbf{e}_\varphi + u_z \mathbf{e}_z$ is the velocity vector, p is the pressure, ρ is the fluid density, μ is the dynamic viscosity.

In cylindrical coordinates, the azimuthal momentum equation takes the form

$$\frac{\partial u_\varphi}{\partial t} + u_r \frac{\partial u_\varphi}{\partial r} + \frac{u_\varphi}{r}\frac{\partial u_\varphi}{\partial \varphi} + u_z \frac{\partial u_\varphi}{\partial z} + \frac{u_r u_\varphi}{r} = \nu\left(\nabla^2 u_\varphi - \frac{u_\varphi}{r^2}\right), \quad (5)$$

where ν is the kinematic viscosity of the fluid.

An intense annular shear layer is formed near the stationary central rod, within which a significant radial gradient of the azimuthal velocity $\partial u_\varphi/\partial r \neq 0$ develops. The principal dimensionless parameter of the flow is the Reynolds number,

$$Re_s = U_\varphi \delta_s / \nu \,, \quad (6)$$

where U_φ is the characteristic azimuthal velocity in the annular layer and δ_s is the characteristic thickness of the annular shear layer.

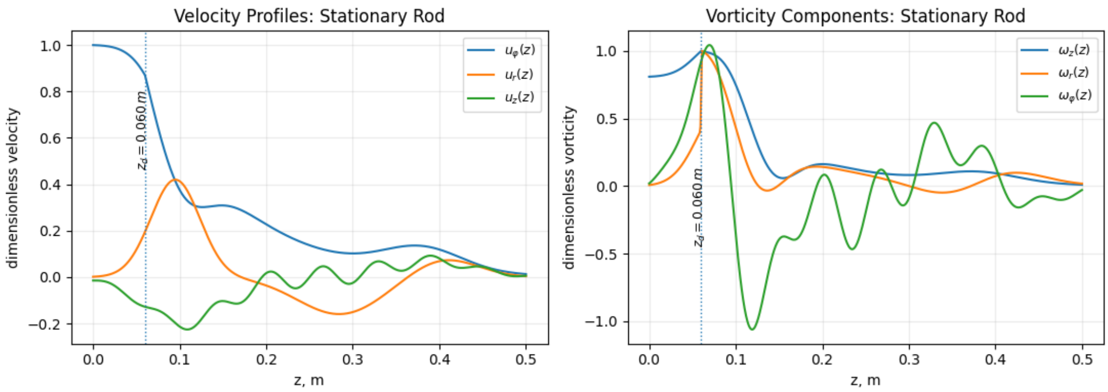

Figure 1. Dimensionless vertical profiles of velocity components and vorticity for a swirling flow in a cylindrical reservoir with a rotating disk and a stationary central rod. The plots demonstrate the influence of the internal obstacle on the redistribution of azimuthal velocity, the formation of the annular shear layer, and the emergence of localized regions of enhanced vorticity near the rod.

When the local Reynolds number reaches critical values $Re_s > Re_{cr}$, the axisymmetric flow loses stability and a non-axisymmetric azimuthal mode $m = 4$ appears within the annular layer. The perturbation field is represented as

$$u'(r, \varphi, z) = A(r, z)\cos(4\varphi - kz) \,, \quad (7)$$

where $A(r, z)$ characterizes the spatial distribution of the mode amplitude and k is the longitudinal wavenumber of the helical structure.

Due to the spatial phase shift, the transverse quadrupole modes merge into a unified helical shell representing a spatially deformed annular layer of angular momentum transport surrounding the stationary central rod.Type equation here.

3.1. Numerical Simulations. Numerical simulations were performed for an incompressible viscous fluid inside a cylindrical reservoir with a rotating disk and a stationary central rod. The computational domain was described in the cylindrical coordinate system (r, φ, z), and the flow field was governed by the incompressible Navier–Stokes equations together with the continuity condition (4). A no-slip boundary condition was imposed at the surface of the rotating disk: $u_\varphi(r, z = 0) = \Omega r$, whereas at the surface of the stationary rod and at the cylindrical sidewall of the reservoir the condition $u_\varphi = 0$ was prescribed. The calculations were carried out for water with kinematic viscosity $\nu = 10^{-6}\, m^2/s$. The geometric parameters of the system were chosen as follows: reservoir radius $R = 0.50\, m$, reservoir height $H = 0.50\, m$, rotating disk radius $b = 0.13\, m$, and central rod radius $r_s = 0.06\, m$. The angular velocity of the disk was set to $\Omega = 100\, rad/s$. To characterize the flow regime, the rotational Reynolds number was introduced: $Re_\Omega = \Omega R^2/\nu$. For the selected parameters, $Re_\Omega \approx 2.5 \times 10^7$, which corresponds to a strongly inertial flow regime in which viscous effects remain important only inside the boundary layers and within the annular shear layer formed near the stationary rod. The thickness of the viscous layer near the rotating disk was estimated using the von Kármán scaling: $\delta \sim \sqrt{\nu/\Omega} \approx 10^{-4} m$. A boundary layer of the same order of magnitude is also formed near the surface of the stationary rod, where a strong radial gradient of azimuthal velocity develops: $\partial u_\varphi/\partial r \neq 0$. The numerical solution was constructed on the basis of an axisymmetric base flow followed by an analysis of spatial perturbations of the form given in equation (7). Vertical profiles of velocity and vorticity components were evaluated along the line $r = r_s + \delta_s$, which passes through the region of maximum shear inside the annular layer.

Figure 1 illustrates the vertical distributions of the dimensionless velocity and vorticity components within the swirling flow near the stationary central rod. The left panel presents the profiles of the velocity components $u_\varphi(z), u_r(z)$ and $u_z(z)$. The azimuthal velocity u_φ reaches its maximum near the rotating disk and gradually decreases with increasing axial coordinate z, reflecting the progressive dissipation and redistribution of angular momentum along the height of the reservoir. The radial velocity component u_r changes sign along the vertical direction, indicating the presence of toroidal recirculation. In the lower part of the reservoir the fluid is transported outward toward the periphery under the action of centrifugal forces, whereas in the upper region a compensating inward motion toward the axis is formed. The axial velocity u_z demonstrates the existence of a downward flow near the rod together with localized recirculation zones associated with the closure of the meridional circulation. The right panel shows the vorticity components $\omega_r(z), \omega_\varphi(z)$ and $\omega_z(z)$. The maximum axial vorticity ω_z is localized near the surface of the stationary rod, where the annular shear layer with the strongest azimuthal velocity gradient is formed. The azimuthal vorticity ω_φ reflects the curvature of the meridional flow and is associated with the formation of secondary recirculation structures. The radial vorticity component ω_r exhibits an alternating-sign behavior caused by the spatial deformation of the annular vortex layer and the development of azimuthal instability modes. The oscillatory character of the vorticity profiles indicates the loss of complete axial symmetry and the onset of a spatially nonuniform helical structure developing around the stationary rod.

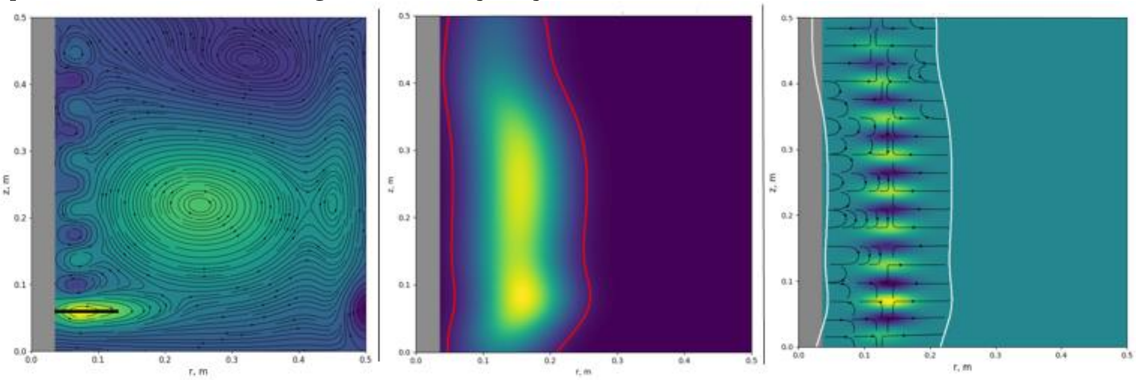

Figure 2. The longitudinal structure of a localized helical mode in a cylindrical reservoir with a stationary central rod. The left panel shows the streamline field and recirculation zones in the (r, z) plane, demonstrating the spatial reorganization of the swirling flow and the formation of localized vortex cells. The central panel presents the region influenced by the helical shell, determined by the distribution of the mode amplitude within the annular shear layer. The right panel shows the localized helical structure with suppression of the outer flow field, reflecting the spatial concentration of vorticity and recirculation zones near the stationary central rod.

4. Spectral Stability and Modal Structure of the Annular Shear Layer.

To determine the spatial structure of the most unstable perturbation, we consider the stability of the annular shear layer formed near the stationary central rod. In the axisymmetric base state, the azimuthal velocity depends only on the radial and axial coordinates r and z:

$$u_\varphi = u_{\varphi 0}(r, z)\,. \tag{8}$$

The principal radial velocity gradient is localized inside the annular layer of thickness δ_s near the surface of the stationary rod $(\partial u_\varphi/\partial r \neq 0)$. To analyze the stability of the flow, the velocity field is represented as the sum of the base flow and a small perturbation:

$$\mathbf{u} = \mathbf{u}_0 + \mathbf{u}'\,, \tag{9}$$

where $\mathbf{u}_0$ corresponds to the mean swirling flow, while $\mathbf{u}'$ describes the spatial modal structure of the perturbation. For the analysis of the spatial instability structure, the perturbation field is expanded into azimuthal Fourier modes:

$$u'(r,\varphi,z,t) = \sum_{m=0}^{\infty} A_m(r,z,t)\exp(im\varphi)\ , \quad (10)$$

where m denotes the azimuthal wave number, while $A_m(r,z,t)$ characterizes the spatial amplitude of the corresponding mode. Such a decomposition makes it possible to represent an arbitrary non-axisymmetric perturbation as a superposition of azimuthal harmonics of different orders.

Each individual harmonic may be represented in the form of a wave-like perturbation:

$$A_m(r,z,t) = \hat{u}_m(r,z)\exp(-i\omega t), \quad (11)$$

where $\omega = \omega_r + i\omega_i$ is the complex frequency. The perturbation field corresponding to an individual mode therefore takes the form $\omega_i > 0$ corresponds to exponential growth of the modal amplitude and indicates hydrodynamic instability of the annular shear layer.

Each value of m corresponds to a specific spatial symmetry of the flow. The mode $m = 0$ describes an axisymmetric state, $m = 1$ corresponds to a one-sided displacement of the vortex structure, and $m = 2$ forms a dipole configuration, whereas $m = 4$ corresponds to a quadrupole structure with four azimuthal regions of enhanced vorticity (Table1)..

Table 1.

Relationship Between Azimuthal Modes and Swirl Intensity

Regime	Most Probable Mode
Weak swirl	$m = 0$
Moderate swirl	$m = 1$
Strong annular shear	$m = 2$
Thin strongly sheared layer	$m = 3 - 4$

Spectral analysis of the velocity and vorticity fields demonstrates that, upon reaching a critical value of the local Reynolds number, the spectrum exhibits pronounced contributions of both the dipole mode $m = 2$ and the quadrupole harmonic $m = 4$. This indicates that the quadrupole perturbation acquires the largest growth rate and becomes the dominant spatial structure of the annular shear layer. As a result, the flow loses complete axial symmetry and reorganizes into a four-lobed helical shell surrounding the stationary central rod.

The presence of a longitudinal phase shift produces an additional spatial modulation:

$$u'(r,\varphi,z) = A(r,z)\cos(4\varphi - kz), \quad (12)$$

where k denotes the axial wave number of the helical structure. This expression describes the spatial rotation of the quadrupole mode along the height of the reservoir and the formation of a helical shell inside the annular shear layer.

Linearization of the Navier–Stokes equations about the base state leads to a spectral stability problem for the annular shear layer. The principal instability mechanism is associated with a combination of centrifugal instability and Kelvin–Helmholtz-type shear instability. For $\Omega = u_\varphi/r$ the necessary condition for instability is determined by the Rayleigh–Fjørtoft criterion:

$$\frac{\partial}{\partial r}\left[\frac{1}{r^3}\frac{\partial(r^2\Omega)}{\partial r}\right] = 0\ . \quad (13)$$

Since the azimuthal velocity profile near the stationary rod possesses a pronounced inflection point, the instability criterion is satisfied inside the annular shear layer. The characteristic azimuthal wave number of the fastest-growing mode is determined by the ratio between the radius of the annular layer and its thickness. For an annular structure with radius r_s and thickness δ_s , the characteristic azimuthal wavelength may be estimated as $\lambda_\varphi \sim 2\pi\delta_s$. The corresponding number of azimuthal modes distributed along the circumference is therefore given by

$$m_* \sim 2\pi r_s/\lambda_\varphi \sim r_s/\delta_s\ . \quad (14)$$

For the flow parameters considered in the present study, the ratio r_s/δ_s is of the order of several units, as a result of which the quadrupole harmonic $m = 4$ becomes clearly observable in the developed nonlinear regime. This mode corresponds to the formation of four azimuthal regions of enhanced vorticity and localized pressure reduction around the stationary rod. The spatial structure of the perturbation is described by equation (7).

Modes with smaller values of m possess insufficient spatial localization and therefore do not provide stable separation of the annular layer, whereas modes with larger m are strongly suppressed by viscous dissipation due to their small azimuthal scales. Consequently, the quadrupole mode represents a compromise between inertial amplification and viscous damping and therefore acquires the maximum growth rate.

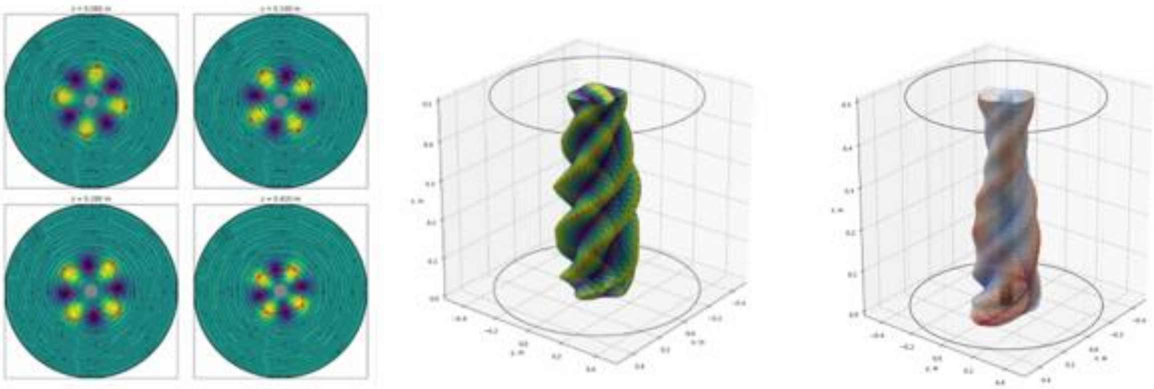

Figure 3. Transverse cross-sections of the quadrupole azimuthal mode and the corresponding spatial helical shell in a cylindrical reservoir with a rotating disk and a stationary central rod. The left panel shows the transverse structures of the mode m = 4, forming four stable convective regions around the rod. The rotation of the structure along the reservoir height reflects the presence of a phase shift $\theta(z) = kz$. The central panel presents the three-dimensional helical shell arising from the spatial connection of the transverse modal structures within the annular shear layer. The right panel shows a mixed helical shell $m = 2 + m = 4$ with a semi-conical expansion in the vicinity of the rotating disk.

As a result, the annular shear layer loses its complete axial symmetry and reorganizes into a spatial quadrupole helical shell surrounding the stationary central rod.

The emergence of this mode leads to the loss of complete axial symmetry of the flow and to the division of the annular vortex layer into four spatially organized regions. In the transverse cross-section of the reservoir, sectors of intensified swirl, locally reduced pressure, enhanced vorticity, and radial momentum transport are formed.

The pressure field may be represented as

$$p(r,\varphi,z) = p_0(r,z) + P_4(r,z)\cos(4\varphi)\,, \quad (15)$$

where $p_0(r,z)$ corresponds to the axisymmetric pressure component and $P_4(r,z)$ describes the amplitude of the quadrupole modulation.

The azimuthal pressure nonuniformity leads to the formation of four stable convective regions around the stationary rod. Within these regions, local recirculation flows and zones of enhanced vorticity develop due to the redistribution of angular momentum inside the annular shear layer. With further development of the swirl, the transverse quadrupole structures acquire a spatial phase shift along the height of the reservoir and transform into a three-dimensional helical shell.

Table 2.

Comparison of Azimuthal Modes of the Annular Shear Layer

Mode m	Spatial Structure	Number of Azimuthal Regions	Stability Characteristics	Physical Interpretation
$m = 0$	Axisymmetric flow	0	Stable at low Re	Uniform annular rotation without spatial deformation
$m = 1$	Single-lobe asymmetry	1	Weakly stable	Displacement of the vortex core relative to the reservoir axis
$m = 2$	Dipole structure	2	Moderately stable	Formation of two opposite regions of intensified swirl
$m = 3$	Three-lobed mode	3	Limited stability	Spatially nonuniform vorticity distribution with increased dissipation
$m = 4$	Quadrupole helical mode	4	Most stable	Formation of four stable channels of angular momentum transport around the rod

As follows from Table 2, the mode $m = 4$ represents an optimal compromise between inertial amplification and viscous dissipation. Modes with smaller values of m possess insufficient spatial localization and do not provide stable separation of the annular shear layer, whereas modes with larger values of m are suppressed by viscous dissipation due to the decreasing azimuthal scale of the perturbations. As a result, for the flow parameters considered in the present study, the quadrupole mode exhibits the largest growth rate and forms a spatial helical shell around the stationary central rod.

4.1 Spectral Structure of Azimuthal Perturbations.

For a more accurate description of the spatial flow structure, it is necessary to take into account that the observed four-lobed pattern may not represent an independent primary $m = 4$ mode, but rather the result of a nonlinear superposition of the fundamental dipole mode $m = 2$ and its second harmonic $m = 4$. In this case, the perturbation field may be written as

$$u'(r, \varphi, z, t) = A_2(r, z, t)\cos(2\varphi - k_2 z - \omega_2 t) + A_4(r, z, t)\cos(4\varphi - k_4 z - \omega_4 t)\ , \quad (16)$$

where the first term describes the large-scale dipolar deformation of the annular shear layer, while the second term represents the quadrupole modulation responsible for the formation of four localized regions of enhanced vorticity around the stationary rod. Such a solution corresponds to a mixed modal state in which the global instability is primarily associated with the $m = 2$ mode, whereas the observed four-sector structure is amplified by the harmonic $m = 4$.

The emergence of the harmonic $m = 4$ naturally follows from the nonlinear terms of the Navier–Stokes equations. If a dipole perturbation is already present in the flow,

$$u'_2 = A_2\cos(2\varphi - k_2 z)\ , \quad (17)$$

then the quadratic inertial term $(\mathbf{u}' \cdot \nabla)\,\mathbf{u}'$ contains the self-product of this mode:

$$\cos^2(2\varphi - k_2 z) = 0.5\,[1 + \cos(4\varphi - 2k_2 z)]\ . \quad (18)$$

Thus, quadratic nonlinear interactions naturally transfer energy from the dipole mode to its second azimuthal harmonic. It follows from this expression that self-interaction of the $m = 2$ mode automatically generates the second harmonic $m = 4$. Therefore, the presence of a quadrupole structure does not necessarily imply that $m = 4$ represents an independent primary instability. Instead, it may arise as a nonlinear harmonic of the dipole instability. In this case, the spectral representation of the perturbation takes the form given by equation (10), while in the developed regime the dominant part of the perturbation energy is concentrated in two azimuthal modes:

$$|A_2| > 0, |A_4| > 0\ , \quad (19)$$

whereas the remaining harmonics possess substantially smaller amplitudes:

$$|A_m| \ll |A_2| + |A_4|\ , m \neq 2, 4 \quad (20)$$

The criterion of the mixed regime is the presence of two pronounced peaks in the azimuthal spectrum of vorticity or velocity:

$$E_m(z) = \left|\int_0^{2\pi} \omega_z(r, \varphi, z)\exp(-im\varphi)d\varphi\right|^2, \quad (21)$$

where E_m denotes the azimuthal spectral energy density of the mode m.

If the spectrum exhibits a maximum at $m = 2$ together with a pronounced second harmonic at $m = 4$, then the observed structure should be interpreted as a superposition $m = 2 + m = 4$. In this case, the four-lobed pattern represents the result of nonlinear amplification of the second harmonic rather than evidence of the primary selection of a purely quadrupole mode.

Thus, the most physically consistent interpretation is that the stationary central rod forms an annular shear layer that initially loses stability through the dipole mode $m = 2$. As the swirl intensity increases, nonlinear self-interaction of this mode generates the harmonic $m = 4$, resulting in the formation of a four-sector spatial structure around the rod. In the presence of a longitudinal phase shift, both modes acquire a helical character, and the perturbation field may be described as a mixed helical shell:

$$u'(r, \varphi, z) = A_2(r, z)\cos(2\varphi - k_2 z) + A_4(r, z)\cos(4\varphi - k_4 z)\ (22)$$

During the development of the dipole mode $m = 2$, the annular shear layer ceases to be azimuthally uniform. In two opposite sectors, a local amplification of the azimuthal velocity gradient and a concentration of vorticity arise. As a consequence of nonlinear advection, these regions undergo additional deformation and localized azimuthal compression. This process leads to a local densification of streamlines and a concentration of angular momentum within individual regions of the annular shear layer.

Since the convective transport term in the Navier–Stokes equations is quadratic, amplification of the dipole structure automatically generates a second azimuthal harmonic. Physically, this corresponds to the splitting of two large-scale vortex regions into four localized sectors of enhanced vorticity. As a result, the initial dipole mode gradually acquires a pronounced quadrupole modulation.

Thus, the $m = 4$ structure does not arise as an independent primary instability, but rather as a consequence of nonlinear redistribution of vorticity and spatial concentration of energy within the dipolar annular shear layer.

5. Formation of the Thin Annular Shear Layer. The rotating disk transfers angular momentum to the fluid, resulting in the formation of an intense swirling motion within the reservoir: $u_\varphi \sim \Omega r$. However, the presence of the stationary central rod suppresses the rotation of the fluid in the axial region. As a consequence, a continuous axial vortex core cannot form, and the flow reorganizes into an annular vortex layer: $r_s < r < r_s + \delta_s$. Within this region, an intense radial gradient of the azimuthal velocity $\partial u_\varphi/\partial r \neq 0$, is generated, becoming the source of azimuthal hydrodynamic instability. The maximum values of the velocity gradient are localized near the surface of the stationary rod, where the azimuthal motion is strongly decelerated due to the no-slip boundary condition $u_\varphi(r_s) = 0$.

Physically, the stationary rod acts as an internal obstacle suppressing the formation of a continuous axial vortex core. As a result, the swirling flow acquires the structure of a hollow vortex shell, within which the primary transport of angular momentum occurs in the annular region between the rod surface and the outer part of the reservoir.

6. Formation of the Helical Shell

Inside the annular shear layer, intense swirl, radial momentum transport, and local concentration of vorticity coexist simultaneously. The axial vorticity is defined as

$$\omega_z = (1/r)\big(\partial(ru_\varphi)/\partial r\big). \quad (23)$$

As the swirl intensity increases, the layer loses complete axial symmetry, leading to the emergence of non-axisymmetric azimuthal modes. Within the considered parameter range, the observed quadrupole structure is interpreted as a mixed modal state involving the dipole mode $m = 2$ and its nonlinear harmonic $m = 4$, leading to the formation of four convective regions around the stationary rod. With further development of the swirl, these transverse structures acquire a spatial phase shift along the height of the reservoir and merge into a coherent helical shell of the deformed annular vortex layer.

The appearance of longitudinal phase modulation means that the maxima of the quadrupole mode become displaced in the azimuthal direction as the coordinate z changes. As a result, the transverse convective regions lose their independence and merge into a unified spatial structure. Individual regions of enhanced vorticity become connected along helical trajectories, forming spatial channels of angular momentum transport. The trajectory of the maxima of the helical shell is determined by

$$\varphi(z) = \varphi_0 + kz + \varphi_m \,, \qquad (24)$$

where φ_0 corresponds to the initial azimuthal position of the mode.

Thus, the transverse quadrupole structure transforms into a spatial helical shell of the deformed annular vortex layer. Unlike classical concentrated helical vortices, the considered shell represents a spatially modulated surface of angular momentum transport localized within the annular shear layer surrounding the stationary central rod.

Inside the helical shell, maximum values of local vorticity, intense radial–azimuthal momentum transport, and reduced pressure are observed. At the same time, the shell preserves its coherence due to the balance between centrifugal forces, pressure gradients, and viscous dissipation. The spatial deformation of the structure is accompanied by the formation of local recirculation regions and secondary toroidal vortex zones interacting with the primary helical flow.

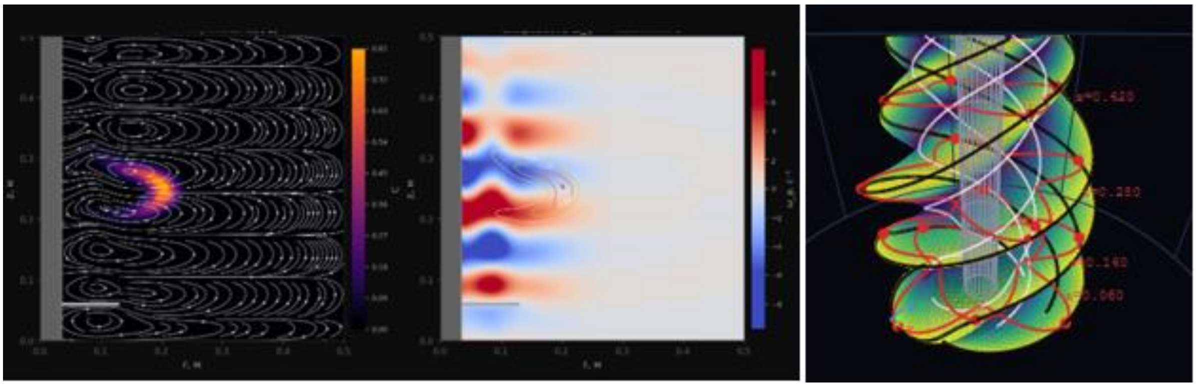

Figure 4. The spatial organization of a quadrupole helical mode in a swirling fluid flow within a cylindrical reservoir with a rotating disk and a stationary central rod. The left panel shows the impurity concentration distribution in a longitudinal cross-section, demonstrating the localization of mass transport inside the helical shell and the formation of closed recirculation zones. The central panel presents the vorticity field and streamlines, illustrating the spatial deformation of the annular shear layer and the emergence of the nonlinear azimuthal mode (1). The right panel depicts the three-dimensional helical shell of the quadrupole mode formed around the stationary rod as a result of the phase shift of transverse structures along the height of the reservoir. The surface color modulation reflects the spatial distribution of swirl intensity and local vorticity within the deformed annular layer of angular momentum transport.

Unlike classical helical vortex filaments, the considered structure does not form a continuous rotating vortex core. The primary transport of angular momentum occurs within the deformed annular shear layer, which spatially envelops the stationary rod and forms a coherent helical shell.

As the distance from the rotating disk increases, the deformation amplitude $A(z)$ decreases due to viscous damping and energy redistribution within the main fluid volume. As a consequence, the helical shell gradually becomes smoother and transitions toward a more axisymmetric spatial state.

7. Internal Force Balance. The stability of the helical shell is determined by the interaction of several hydrodynamic mechanisms. The principal role is played by the balance between centrifugal forces, pressure gradients, viscous dissipation, and the spatial curvature of streamlines inside the annular vortex layer.

Due to the intense azimuthal motion within the shell, centrifugal forces arise that tend to expand the vortex structure in the radial direction:

$$F_c = \rho\left(u_\varphi^2/r\right). \qquad (25)$$

This radial expansion is counteracted by the radial pressure gradient,

$$\partial p/\partial r = \rho\left(u_\varphi^2/r\right), \qquad (26)$$

as a result of which a self-consistent pressure field is formed inside the shell. Thus, the spatial structure is maintained not by geometric confinement alone but by the internal balance between centrifugal expansion and pressure gradients. This gives the helical shell the properties of an internally organized coherent hydrodynamic structure. An additional role is played by viscous interaction. On the surface of the stationary rod, the no-slip condition: $u_\varphi(r_s) = 0$ is satisfied, whereas inside the annular layer the azimuthal velocity remains substantial. Consequently, an intense shear stress arises:

$$\tau_{r\varphi} = \mu\left(\partial u_\varphi/\partial r\right) \qquad (27)$$

which tends to smooth azimuthal nonuniformities and restore the axisymmetric flow state. Viscosity therefore acts as a dissipation mechanism reducing the amplitude of the spatial mode. At the same time, the rotating disk continuously supplies angular momentum to the system:

$$M \sim \rho\Omega^2 b^5 \qquad (28)$$

where Ω is the angular velocity of the disk and b is its radius. As a result, a dynamic balance is established inside the reservoir between energy input and viscous dissipation. As long as this balance is maintained, the helical shell remains stable.

A significant influence is also exerted by the spatial curvature of the helical structure. Since the streamlines are curved along helical trajectories, additional inertial stresses arise inside the shell:

$$\sigma_i \sim\rho(u_s^2/R_c), \quad (29)$$

where u_s is the velocity along the helical streamline and R_c is the local radius of curvature of the shell. These inertial stresses tend to straighten the helical structure and reduce its spatial curvature. However, the spatial azimuthal mode simultaneously generates alternating regions of reduced and elevated pressure, producing a self-consistent force distribution that maintains the shell geometry. An important role is also played by the vorticity balance, $\boldsymbol{\omega} = \nabla \times \mathbf{u}$. Inside the annular layer, a local concentration of vorticity is observed, although its accumulation is limited by spatial redistribution processes. Part of the vorticity is transported upward along the helical channels, part is dissipated by viscosity, and part becomes involved in secondary toroidal recirculation structures. As a consequence, the helical shell continuously exchanges momentum and vorticity with the surrounding fluid volume while preserving its coherent spatial organization.

8. Secondary Toroidal Structures. The spatial helical shell causes pressure redistribution throughout the reservoir volume, resulting in the formation of secondary toroidal recirculation zones within the flow. In this case, the pressure field may be represented as

$$p = p_0 + P_4\cos(4\varphi - kz) + P_t(r,z) \quad (30)$$

where p_0 corresponds to the axisymmetric pressure component, P_4 characterizes the azimuthal modulation associated with the quadrupole mode, and, $P_t(r,z)$ describes the additional pressure induced by the secondary toroidal flows.

Toroidal structures are formed in regions where a longitudinal pressure gradient, $\partial p/\partial z \neq 0$ appears. In these zones, closed circulation contours arise: $\oint \mathbf{u}\cdot d\mathbf{l} \neq 0$, corresponding to localized fluid recirculation regions.

The formation of toroidal structures is associated with the spatial nonuniformity of the helical shell and with the redistribution of angular momentum along the reservoir height. In regions of reduced pressure, the flow is drawn into the helical channels, whereas in regions of elevated pressure a reverse fluid motion develops.

As a consequence, a system of closed toroidal circulations interacting with the primary swirling flow is formed inside the reservoir. The toroidal recirculation zones modify the local distributions of velocity, pressure, and vorticity, and also influence impurity transport and the spatial stability of the helical shell. Within these regions, additional local potential zones arise in which the fluid may perform long-term circulatory motion around the helical structure.

9. Impurity Transport. The motion of a dye droplet inside the swirling flow in a cylindrical reservoir with a rotating disk and a stationary central rod is considered. After being introduced into the flow, the droplet is initially entrained into the primary rotational motion of the fluid and begins to move around the rod under the action of the azimuthal velocity component. Its trajectory is determined by the superposition of the azimuthal, radial, and axial velocity components defined in Eq. (3).

At the initial stage of motion, the droplet rapidly acquires azimuthal velocity:

$$d\varphi/dt = u_\varphi/r \approx \Omega \quad (31)$$

and begins to rotate around the central rod. Simultaneously, centrifugal forces generate radial fluid transport:

$$dr/dt = u_r\,, F_c = \rho\left(u_\varphi^2/r\right)\,, \quad (32)$$

as a result of which the droplet trajectory ceases to be circular and acquires a spiral form. In the lower part of the reservoir, where the influence of the rotating disk is maximal, the droplet moves along an expanding helical trajectory:

$$dr/dt > 0, d\varphi/dt = u_\varphi/r \quad (33)$$

As the droplet approaches the stationary rod, the flow decelerates due to the no-slip condition $u_\varphi(r_s) = 0$. Consequently, an annular shear layer is formed around the rod:

$$\partial u_\varphi/\partial r \neq 0\,, \quad (34)$$

within which the droplet undergoes intense stretching and deformation along the streamlines. Entering the region of the helical shell, the droplet begins to follow the spatial geometry of the modal structure. Its trajectory acquires the form of a helical line:

$$\varphi(z) = \varphi_0 + kz, \quad (35)$$

where k is the longitudinal wavenumber of the helical mode.

If the flow remains stable, the droplet motion becomes localized inside one of the four azimuthal channels of the quadrupole mode described by

$$u'(r,\varphi,z) = A(r,z)\cos(4\varphi - kz). \quad (36)$$

In regions of reduced pressure,

$$p(r,\varphi,z) = p_0(r,z) + P_4(r,z)\cos(4\varphi - kz) \quad (37)$$

the droplet accelerates and is drawn into the helical shell, whereas in regions of elevated pressure its motion slows down. As a result, the trajectory becomes spatially nonuniform: along the helical structure the droplet periodically accelerates and decelerates.

As the droplet propagates upward through the reservoir, it becomes involved in the spatial circulation of the flow. Part of the impurity is transported upward along the helical channels and may subsequently become entrained into secondary toroidal recirculation zones. Within such regions, closed circulation contours arise:

$$\oint \mathbf{u}\cdot d\mathbf{l} \neq 0\,, \quad (38)$$

corresponding to repeated circulatory fluid motion around the helical shell.

If the droplet enters the interaction region between the helical shell and a secondary toroidal vortex, the trajectory acquires a complex spatial structure. The motion then consists of two superposed rotations: a rapid azimuthal motion around the rod and a slower toroidal transport along closed recirculation contours. As a consequence, the trajectory assumes the form of a spatial epicycloidal spiral.

Over time, the droplet is stretched due to shear stresses:

$$\tau = \mu(\partial u_\varphi/\partial r) \ , \quad (39)$$

causing the initially compact impurity region to transform into a thin helical filament re- producing the geometry of the vortex shell. The further evolution of the impurity is governed by the combined action of advection and diffusion and is described by the transport equation

$$(\partial C/\partial t) + (u\cdot\nabla)C = D\nabla^2 C \ , \quad (40)$$

where $C(r,\varphi,z,t)$ is the dye concentration and D is the coefficient of molecular diffusion.

At the initial stage, advective transport dominates:

$$(u\cdot\nabla)C \gg D\nabla^2 C \ , \quad (41)$$

therefore the impurity is stretched into a long helical structure whose shape is determined by the geometry of the vortex shell and the secondary recirculation zones. At later stages, diffusive smoothing becomes increasingly important, causing the concentration to gradually equalize throughout the reservoir volume

Thus, impurity transport in the considered flow is governed by the spatial organization of the swirling motion. The droplet is successively entrained into the primary rotation, drawn into the helical shell surrounding the stationary rod, interacts with secondary toroidal structures, and gradually transforms into a complex three-dimensional helical concentration structure.

10. r–z Cross-Section: Longitudinal Structure (Fig. 2a and 4a). In the axisymmetric base state, $\partial/\partial\varphi = 0$ and Eq. (5) reduces to the diffusion–convection transport equation for the angular velocity $\Omega(r,z) = u_\varphi/r$:

$$\frac{\partial\Omega}{\partial t} + u_r\frac{\partial\Omega}{\partial r} + u_z\frac{\partial\Omega}{\partial z} = \nu\left[\frac{\partial^2\Omega}{\partial r^2} + \frac{3}{r}\frac{\partial\Omega}{\partial r} + \frac{\partial^2\Omega}{\partial z^2}\right] \quad (42)$$

The operator containing the coefficient $3/r$ in front of the first radial derivative reflects not the diffusion of a scalar quantity but the diffusion of angular momentum $L = r^2\Omega$, for which the equation may be rewritten as

$$\frac{\partial L}{\partial t} + u_r\frac{\partial L}{\partial r} + u_z\frac{\partial L}{\partial z} = \nu\left[\frac{\partial^2 L}{\partial r^2} + \frac{3}{r}\frac{\partial L}{\partial r} + \frac{\partial^2 L}{\partial z^2}\right] \quad (43)$$

This clearly demonstrates that angular momentum L transport is suppressed by the centrifugal term, causing angular momentum to concentrate near the outer wall, while a sharp radial velocity gradient forms near the rod. The meridional flow (u_r, u_z) is determined from the continuity condition

$$(\partial(ru_r)/\partial r) + r(\partial u_z/\partial z) = 0 \quad (44)$$

together with the momentum equations for the radial and axial velocity components.

Near the rotating disk, a von Kármán layer develops: the fluid is spun up by the disk, centrifugal forces eject it radially outward, and the axial pressure gradient generates a compensating downward axial inflow. Along the axis (or near the rod), a descending flow is formed with a characteristic velocity of the order $u_z \sim -\nu^{1/2}\Omega_d^{1/2}$, which reaches its maximum inside the von Kármán layer and decreases according to a power law with increasing distance from the disk. Outside the annular shear layer, a weak upward recirculation develops, closing the meridional circulation cell. Consequently, the dependence $u_z(r)$ becomes sign−changing: near r_s a negative minimum is observed, whereas for $r > r_s$ the velocity becomes weakly positive.

Radial momentum transport also exhibits a dual structure. Near the upper boundary, tangential injection produces a weak inward-directed flow: the fluid acquires swirl and slowly drifts toward the axis. Near the bottom, in contrast, a weak outward radial flow develops. Therefore, impurity particles introduced from above experience both axial descent and a slow inward radial drift, making their trajectories fundamentally different from purely vertical settling.

The azimuthal velocity field inside the annular layer is well approximated by

$$u_\varphi(r,z) = U_0 f(z) g(r) \ , \quad (45)$$

where $f(z) = (z/H)^\alpha, g(r) = \tanh((r - r_s)/\delta_s)$. The function $f(z)$ describes the weakening of the disk influence with height ($\alpha \approx 0.5 - 1$), a $g(r)$ models a shear layer of thickness δ_s. The radial shear reaches its maximum at $r = r_s$:

$$\left.\frac{\partial u_\varphi}{\partial r}\right|_{r=r_s} = \frac{U_0 f(z)}{\delta_s} \ . \quad (46)$$

The key stability parameter is the Reynolds number of the layer $Re_s = U_0\,\delta_s/\nu$. When the critical value $Re_s^* \approx 150 - 300$ is exceeded, the axisymmetric flow becomes unstable with respect to azimuthal perturbations.

The stability of the annular layer is governed by the competition between centrifugal forces and Kelvin–Helmholtz-type shear instability. A necessary instability condition is given by the generalized Rayleigh–Fjørtoft criterion:

$$\frac{\partial}{\partial r}\left[\frac{1}{r^3}\frac{\partial(r^2\Omega)}{\partial r}\right] = 0. \quad (47)$$

This condition implies the presence of an inflection point in the circulation distribution. In the considered annular layer, such an inflection point exists by construction and is localized near r_s; therefore, azimuthal modes $m = 1, 2, 3.$ arise at sufficiently large Reynolds numbers. For typical parameters, the dominant nonlinear modal state involves the dipole mode m=2 together with its second harmonic $m = 4$.

The growth of this mode is described as a small perturbation of the base flow:

$$u_\varphi(r,\varphi,z,t) = U_0(r,z) + \varepsilon\,\hat{u}_\varphi(r,z)\cos(m\varphi - \omega t) \ , \quad (48)$$

where the complex frequency $\omega = \omega_r + i\omega_i$ has a positive imaginary part $\omega_i > 0$ in the unstable region. The eigenfunction $\hat{u}_\varphi(r,z)$ is localized near r_s and decays exponentially on both sides of the layer. Along the axis, it forms a standing or weakly traveling wave with axial wavenumber k_z, while the phase velocity $c_{ph} = \omega_r/m$ is close to the mean azimuthal velocity inside the layer. It is precisely this spatially periodic structure that forms the observed "shell." The constant-amplitude surface of the perturbation is described as a deformed cylinder:

$$r_{shell}(\varphi,z) = r_s + A\cos[m(\varphi - k_z z)] \ , \quad (49)$$

where $k_z = \pi/Hn$ for an integer number of half-waves n along the reservoir height. In the $r - z$ cross-section, after averaging over φ, only the envelope of this structure is observed - two nearly vertical bands located on both sides of r_s within which vorticity is concentrated.

For an axisymmetric flow, the vertical vorticity component is

$$\omega_z = (1/r)\left(\partial\left(ru_\varphi\right)/\partial r\right), \quad (50)$$

while the azimuthal component is

$$\omega_\varphi = (\partial u_r/\partial z) - (\partial u_z/\partial r). \quad (51)$$

For the profile

$$g(r) = \tanh((r - r_s)/\delta_s) \quad (52)$$

one obtains

$$\omega_z(r) \approx (U_0 f(z)/\delta_s)\,\mathrm{sech}^2((r - r_s)/\delta_s), \quad (53)$$

that is, a function possessing a sharp maximum at r_s and a characteristic width of order δ_s.

The total circulation flux through a horizontal cross-section,

$$\Gamma = \oint u_\varphi dl = 2\pi r\, u_\varphi \quad (54)$$

decreases with increasing distance from the disk due to viscous dissipation and axial transport:

$$\frac{\partial\Gamma}{\partial z} = \nu r \frac{\partial}{\partial r}\left[\frac{1}{r}\frac{\partial(ru_\varphi)}{\partial r}\right]\frac{r}{u_z} \quad (55)$$

This corresponds to the gradual spreading of the annular vortex layer as the fluid is transported upward.

The velocity vectors in the r-z cross-section reflect the meridional circulation: inside the annular layer $(r \approx r_s)$, the vector (u_r, u_z) is directed downward and slightly inward, forming a descending spiral. Outside the layer $(r > r_s)$, a weak upward motion develops, closing the toroidal circulation cell. Near the rod, the pressure is reduced because of the centrifugal deficit; therefore, a weak descending flow usually persists directly along the rod surface.

The combination of these processes forms the observed pattern: a vertically elongated closed vortex layer with radius r_s, a descending core, and an ascending periphery. It is precisely along this descending spiral trajectory that a passive impurity introduced from above is transported toward the disk while simultaneously spreading azimuthally due to molecular and turbulent diffusion.

11. Diffusion and circulation (numerical calculation).

The constructed model considers an axisymmetric viscous flow of an incompressible fluid in a cylindrical reservoir with a stationary sidewall and central rod, a rotating disk at the bottom end, and tangential fluid injection at the upper boundary. The main tool for describing the meridional flow is the stream function $\psi(r, z)$, introduced from the incompressibility condition $\nabla \cdot \mathbf{u} = 0$. In cylindrical coordinates, the continuity equation is written as follows:

$$(1/r)(\partial(ru_r)/\partial r) + (\partial u_z/\partial z) = 0 \quad (56)$$

This equation is automatically satisfied if the velocity components are defined through the stream function as:

$$u_r = (1/r)(\partial\psi/\partial z), u_z = -(1/r)(\partial\psi/\partial r) \quad (57)$$

With this definition, each line $\psi = const$ represents a streamline of the meridional flow in the (r, z) plane. The specific form of the stream function is chosen as follows:

$$\psi(r, z) = Ar^2(1 - r)[\sin(\pi z/H)(1 + 0.6\sin(2\pi z/H))](1 + 0.4\exp(-z/0.08)) \quad (58)$$

The first factor, $r^2(1 - r)$ ensures that ψ becomes zero both on the rod surface at $r = r_{rod}$, and on the outer wall at $r = R$, which corresponds to the no-slip condition on solid boundaries. The maximum of this polynomial is reached at $r = 2R/3$, that is, approximately in the middle part of the gap between the rod and the wall. This position determines the radial coordinate of the center of the main toroidal recirculation cell. The second factor, containing the first and second harmonics in z, $\sin(\pi z/H)(1 + 0.6\sin(2\pi z/H))$, shifts the maximum of the stream function to the lower third of the reservoir. Numerically, the maximum is reached near $z \approx 0.28H$, which reflects the physical influence of the rotating disk. Through the Kármán layer, the disk creates an intense radial outflow of fluid and forms a downward axial flow along the rod.

The third factor, $\exp(-z/0.08)$ enhances the stream function near the lower endwall, simulating the intensified meridional motion in the Kármán layer of thickness $\delta_K \sim (\nu/\Omega)^{1/2}$, where ν is the kinematic viscosity and Ω is the angular velocity of the rotating disk.

The meridional velocity components are calculated numerically using the central difference scheme:

$$u_r(r, z) = \frac{1}{r}\frac{\psi(r, z+\varepsilon) - \psi(r, z-\varepsilon)}{2\varepsilon}$$
$$u_z(r, z) = -\frac{1}{r}\frac{\psi(r+\varepsilon, z) - \psi(r-\varepsilon, z)}{2\varepsilon} \quad (59)$$

where $\varepsilon = 10^{-4}$ in normalized units. Such a velocity field satisfies the continuity equation with machine precision, since it is constructed as an exact differential of the stream function.

Inside the recirculation cell, the fluid moves along closed toroidal orbits. Near the rotating disk, the fluid is spun up and, under the action of centrifugal force, is thrown toward the wall; it then rises upward along the outer boundary, turns in the upper part of the reservoir, and descends back along the rod. The trajectories are determined by the condition $\psi = const$, while the local velocity along the orbit is proportional to $|\nabla\psi|/r$. The azimuthal velocity component is specified separately in the form

$$u_\varphi(r, z) = \Omega R\mathrm{B}[1 - 0.6\mathrm{B}]\exp\left(-z/z_{decay}\right), \quad (60)$$

where $\mathrm{B} = (r - r_{rod})/(R - r_{rod})$ is the dimensionless normalized radial coordinate inside the annular gap between the central rod and the outer wall of the reservoir, r is the current radial position of the flow point, r_{rod} is the radius of the central rod, and R is the inner radius of the outer wall of the reservoir; $z_{decay} = H(0.3 - 0.025\Omega)$ is the characteristic decay scale of the rotational influence along the vertical direction

At $r = r_{rod}$, the no-slip condition $u_\varphi = 0$ is satisfied, while at $r = R$ the velocity approaches a constant value specified by the tangential fluid injection. The quadratic radial profile corresponds to Couette flow with a correction for the centrifugal redistribution of angular momentum. At Reynolds numbers $Re = U_s\delta_s/\nu$ of the order of several hundred, the profile acquires a characteristic inflection in the region of maximum shear $\partial u_\varphi/\partial r$, located near the radius r_s.

The streamlines are constructed by numerical integration of the system

$$dr/ds = u_r(r, z), dz/ds = u_z(r, z) \quad (61)$$

using the fourth-order Runge–Kutta method with a step size $ds = 0.003$. From each starting point (r_0, z_0) a trajectory of up to 2000 steps is integrated. The integration is terminated when the boundary of the domain is reached or when the streamline closes upon itself:

$$|\delta r|^2 + |\delta z|^2 < 10^{-4} \quad (62)$$

The set of obtained curves forms a structure visually analogous to experimental patterns of meridional flow: a single large toroidal cell with its center located near $r_c \approx 0.3R, z_c \approx 0.28H$, densely filled with closed orbits inside and radial trajectories near the periphery.

The vortex (velocity) map in the background displays the normalized field $u_\varphi/u_{\varphi,max}$ where the dark blue color corresponds to an almost zero velocity near the rod and the upper boundary, while the turquoise-green color represents the maximum azimuthal velocity near the outer wall. This map reflects the distribution of the rotational kinetic energy dissipated in the annular shear layer. The viscous dissipation power is given by

$$\varepsilon_{diss} = \nu \left[r \frac{\partial}{\partial r}\left(\frac{u_\varphi}{r}\right)\right]^2 \quad (63)$$

integrated over the volume. The motion of a passive admixture is described by the advection–diffusion equation:

$$\frac{\partial C}{\partial t} + u_r \frac{\partial C}{\partial r} + u_z \frac{\partial C}{\partial z} = D\left[\frac{1}{r}\frac{\partial}{\partial r}\left(r\frac{\partial C}{\partial r}\right) + \frac{\partial^2 C}{\partial z^2}\right] \quad (64)$$

where D is the molecular diffusion coefficient and C is the admixture concentration. In the Lagrangian formulation, the trajectory of each particle satisfies the equations

$$dr/dt = u_r(r,z) + \xi_r, dz/dt = u_z(r,z) + \xi_z \quad (65)$$

where ξ_r and ξ_z are Gaussian random increments with variance $\sigma^2 = 2D\,dt$, modeling molecular diffusion. The integration is performed using the fourth-order Runge–Kutta method with the subsequent addition of the stochastic contribution. Particles are introduced at the upper boundary of the reservoir at $z = H, r_0 = r_{rod} + 0.45R$, with a small random spread $\delta r \sim 0.02R$. After injection, they are captured by the meridional circulation and move inside the recirculation cell, gradually dispersing due to diffusion. The characteristic residence time of a particle inside the cell is estimated as $\tau_{cell} \sim H/|u_z|_{max}$, which, for typical parameters, amounts to several seconds. During this time, the diffusive spreading has a scale $\ell_{diff} \sim (D\,\tau_{cell})^{1/2}$. For $D = 8 \times 10^{-4}$ and $\tau_{cell} \sim 5\;sec$, we obtain $\ell_{diff} \sim 0.06R$, which is of the same order as the thickness of the annular shear layer δ_s.

12. Boundary of Influence of the Helical Shell. The boundary of influence of the helical shell is defined as the region within which the amplitude of the azimuthal mode remains comparable to the intensity of the main swirling flow. Within this zone, the helical structure significantly modifies the distributions of velocity, pressure, and vorticity, whereas outside it the flow gradually returns to a quasi-axisymmetric rotational state.

The velocity field is represented as a superposition of the mean swirling flow and a spatial modal disturbance:

$$\mathbf{u} = \mathbf{u}_0 + \mathbf{u}' . \quad (66)$$

Here, $\mathbf{u}_0$ corresponds to the main axisymmetric rotational motion, while $\mathbf{u}'$ describes the helical azimuthal mode, $u'(r,\varphi,z) = A(r,z)\cos(4\varphi - kz)$. The amplitude of the modal disturbance is maximal inside the annular shear layer and decreases with distance from it. The radial distribution of the amplitude is approximated by

$$A(r,z) = A_0(z)\exp\left[-\left(r - r_0(z)\right)^2/2\sigma_s^2\right], \quad (67)$$

where $r_0(z)$ is the mean radius of the helical shell, and σ_s is the characteristic thickness of the region influenced by the mode. The strongest effect of the helical structure is observed at $r \approx r_0(z)$, where the main velocity gradients and maximum vorticity values are localized. With increasing distance from this region, the modal amplitude rapidly decreases: $A(r,z) \to 0$. The boundary of influence is defined by the condition under which the energy of the modal disturbance becomes small compared with the energy of the main flow: $|u'|/|u_0| \le \varepsilon$, where $\varepsilon \ll 1$. Typically, $\varepsilon \sim 0.05 - 0.1$. Then the radius of the influence region is determined by the condition

$$A(r_b, z) = \varepsilon A_{max}(z) , \quad (68)$$

from which, for a Gaussian amplitude distribution, one obtains:

$$r_b(z) = r_0(z) + \sigma_s\sqrt{2\ln(1/\varepsilon)} \quad (69)$$

The obtained surface forms a spatial boundary within which the flow retains the influence of the helical mode. Inside this region, the flow is characterized by pronounced azimuthal nonuniformity:

$$\partial u_\varphi/\partial r \neq 0, \partial p/\partial\varphi \neq 0, \omega_z \neq const. \quad (70)$$

Within the region of influence, the azimuthal modulation of pressure, the spatial deformation of streamlines, local pressure minima, and increased vorticity concentration are preserved.

Beyond this boundary, the influence of the helical shell rapidly weakens. In this case, the flow gradually returns to the mean swirling motion: $\mathbf{u}(r,\varphi,z) \approx \mathbf{u}_0(r,z)$, the azimuthal pressure gradients decrease, $\partial p/\partial\varphi \to 0$, and the streamlines become close to concentric circles. Physically, this boundary corresponds to the region where the vortex energy of the helical mode decays. Inside it, the flow remains coupled to the annular shear layer near the stationary rod, whereas outside it the global circulation of the reservoir dominates. Since the helical shell possesses a spatial spiral geometry,

$$\varphi(z) = \varphi_0 + kz , \quad (71)$$

the boundary of its influence also takes the form of a spatial helical surface. This surface is not a cylinder of constant radius and deforms along the reservoir height due to variations in the thickness of the shear layer, the influence of inlet and outlet flows, pressure redistribution, and the gradual decay of vorticity.

Thus, the region influenced by the helical shell represents a spatial annular volume surrounding the stationary rod, within which a coherent helical organization of the flow is maintained. Outside this volume, the helical mode gradually decays, and the flow transitions to a more homogeneous swirling state.

13. Vertical Transformation of the Quadrupole Helical Mode. In the lower part of the reservoir near the rotating disk, the most energetically saturated region of the swirling flow is formed. It is precisely here that the flow receives the maximum angular momentum, as a result of which the circumferential velocity reaches its highest values: $u_\varphi \sim \Omega r$. In this region, an intense annular shear layer develops near the stationary central rod, where the condition $\partial u_\varphi/\partial r \neq 0$ is satisfied.

High velocity gradients lead to an increase in inertial stresses, $\sigma_i \sim \rho(u_s^2/R_c)$, as a result of which the helical structure in the lower part of the reservoir undergoes pronounced nonlinear deformation. The lobes of the quadrupole mode become elongated, the spatial curvature of the streamlines increases, and the outer surface of the shell begins to experience radial oscillations. In this zone, the flow is characterized by maximum vorticity and the most intense pressure redistribution. Pressure minima are concentrated inside the helical channels, leading to local acceleration of the fluid motion and enhanced spatial swirling.

In the lower part of the reservoir, the spatial structure is characterized by a high amplitude of azimuthal modulation described by expression (1), while the function $A(r, z)$ reaches its maximum at small values of the coordinate z. The intense energy input from the rotating disk leads to the formation of pronounced radial-azimuthal flows that enhance the nonlinear deformation of the helical shell. In this region, the quadrupole mode possesses the maximum spatial curvature and the strongest deviation from the axisymmetric state. As the distance from the rotating disk increases and the flow moves upward through the reservoir, the intensity of the swirl gradually decreases. Viscous dissipation and redistribution of angular momentum lead to a reduction in the amplitude of the azimuthal mode: $A(r, z) \downarrow$. At the same time, the local vorticity decreases:

$$\omega_z = (1/r)\left(\partial\left(ru_\varphi\right)/\partial r\right). \quad (72)$$

The upper region of the reservoir is characterized by a smoother and more stable geometry of the helical shell. The spatial structure retains the quadrupole symmetry $m = 4$; however, the deformation of the lobes decreases, and the phase lines become smoother. In this zone, the local curvature of the shell decreases, inertial stresses are reduced, and the radial-azimuthal exchange of momentum weakens. The flow gradually transitions to a more relaxed state, close to a stationary coherent helical mode.

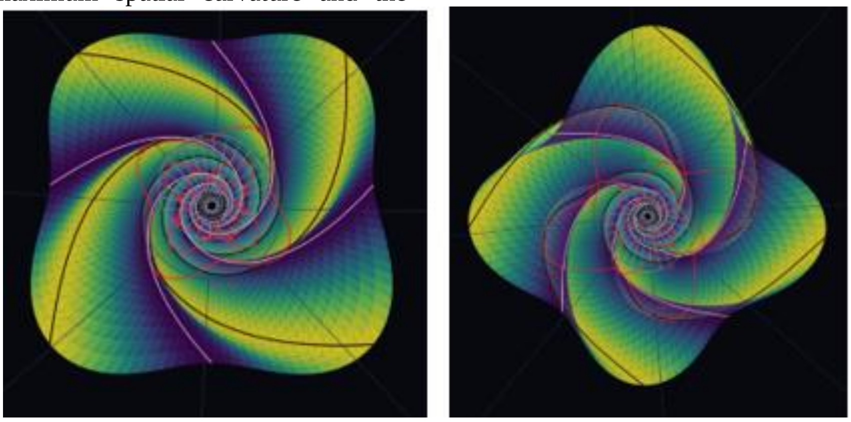

Figure 5. Nonlinear deformation of the quadrupole helical mode in the cross section of the annular swirling layer. Spatial configurations of the azimuthal mode $m = 4$, corresponding to different levels of nonlinear deformation of the helical shell, are shown. The color structure reflects the distribution of swirl intensity and local vorticity, while the spiral lines demonstrate the spatial redistribution of angular momentum inside the deformed annular layer surrounding the stationary central rod.

Since the spatial phase shift $\theta(z) = kz$ (73) is preserved throughout the entire height of the reservoir, the transverse quadrupole structures remain interconnected by a unified helical geometry. However, the intensity of this coupling decreases with increasing distance from the region of maximum energy input. As a result, the lower part of the reservoir corresponds to a regime of strong nonlinear deformation of the shell, whereas the upper region is characterized by a more stable and more symmetric spatial organization of the flow.

Thus, the helical shell is formed in the lower part of the reservoir as an energetically saturated nonlinear structure with a high concentration of angular momentum and intense spatial swirl. Then, as it propagates upward, it gradually loses part of its energy, becomes smoother, and transitions to a more stable spatial state (Fig. 5).

14. Criteria for the Onset and Breakdown of the Mode. The onset of the quadrupole azimuthal mode occurs when the local Reynolds number reaches the critical value $Re_s \geq Re_{s,cr}$. In this region, the flow loses complete axial symmetry, and a stable quadrupole structure with $m = 4$ develops inside the annular vortex layer. The formation of the mode is associated with the development of an azimuthal instability in the region of maximum radial gradients of the circumferential velocity, $\partial u_\varphi/\partial r \neq 0$. With a further increase in the swirl intensity, the quadrupole mode acquires a spatial phase shift along the reservoir height, as a result of which the transverse structures merge into a single helical shell.

Within the range of moderate Reynolds numbers, the helical structure retains its coherence due to the balance between angular momentum input, pressure gradients, and viscous dissipation. In this regime, the flow is characterized by a stable spatial organization and the existence of stationary helical channels for momentum transport. With a further increase in the local Reynolds number, $Re_s \gtrsim 10^4$ the helical shell begins to lose stability. Longitudinal oscillations, local phase shifts, and unsteady deformations of the shell arise within the structure. The spatial coherence is gradually disrupted, after which the shell breaks up into separate unsteady vortex tubes and localized vortex structures.

The breakdown of the shell is accompanied by an intensification of three-dimensional velocity fluctuations, enhanced turbulent mixing, and the appearance of spatially disordered vortex regions. In this regime, the flow undergoes a transition from an organized helical mode to a complex unsteady swirling flow.

The evolution of the structure with increasing swirl intensity may be represented by the following sequence: axisymmetric cross section → $m = 4$ → helical shell → $\mathrm{precession}$ → vortex chaos. Thus, the quadrupole helical mode exists within a limited range of parameters, inside which a balance is maintained between the mechanisms of swirl generation, spatial modulation of the vortex layer, and viscous energy dissipation.

15. Additional Analysis of the Spatial Structure.. In the considered regime, the swirling flow possesses a pronounced spatial organization. The forming helical shell is not an isolated concentrated vortex, but rather a spatially deformed annular layer of angular momentum transport localized around the stationary central rod. As the swirl intensity increases inside the reservoir, stable regions of local accumulation of kinetic energy, enhanced vorticity, and reduced pressure arise. These regions merge into helical channels associated with the quadrupole azimuthal mode.

The spatial geometry of the shell is determined by the phase shift of the transverse modes along the reservoir height. As a consequence, neighboring horizontal cross sections become rotated relative to one another, while the maxima of swirl connect into continuous helical lines. Such an organization of the flow corresponds to a standing helical mode within a confined cylindrical volume, inside which a coherent spatial coupling between the transverse quadrupole structures is maintained.

Inside the helical shell, intense transport of energy and momentum takes place. Centrifugal forces tend to expand the annular vortex layer, whereas pressure gradients and viscous stresses confine the structure to a limited region near the stationary rod. As a result, a dynamic balance is formed between the angular momentum input from the rotating disk and viscous energy dissipation inside the shear layer.

A special role is played by the interaction of the helical shell with secondary toroidal recirculation zones. These structures arise due to pressure redistribution along the reservoir height and lead to the formation of local closed circulation contours. Consequently, a complex system of interconnected vortex structures of different spatial scales is formed inside the reservoir.

The distribution of a passive admixture in the considered flow also acquires a spatially organized character. The injected dye is stretched along the helical channels and forms thin spiral concentration filaments. The transport rate of the admixture is determined not only by the global rotation of the fluid, but also by the local geometry of the azimuthal modes and the secondary recirculation zones.

Of additional interest is the relationship between the observed structure and wave regimes in swirling flows. The spatial organization of the shell resembles a standing-wave configuration in cylindrical resonant systems. The pressure field contains stable azimuthal maxima and minima, while the structure itself possesses a pronounced modal organization and retains coherence within a limited range of flow parameters.

The obtained results make it possible to regard the helical shell as a coherent hydrodynamic structure arising from the loss of complete axial symmetry of the annular shear layer near the stationary central rod. The spatial organization of the flow is determined by the combined action of swirl, viscosity, pressure gradients, and the geometric confinement created by the internal stationary obstacle.

16. Discussion. The obtained results demonstrate that the presence of a stationary central rod radically alters the structure of the swirling flow in a cylindrical reservoir. Instead of forming a continuous axial vortex core, an annular shear layer arises which, at sufficiently large values of the local Reynolds number, becomes a source of azimuthal instability.

A distinctive feature of the considered regime is the formation of a stationary quadrupole mode with $m = 4$. Unlike classical Taylor–Couette vortices, the observed structure is not associated with the formation of periodic annular vortices between rotating cylinders. In the present configuration, a spatial deformation of a hollow vortex shell around a stationary internal obstacle develops. The main transport of angular momentum occurs within a confined annular layer, which loses complete axial symmetry and transitions to a spatially nonuniform state.

The obtained structure possesses several properties of a coherent hydrodynamic mode. It is characterized by spatial phase synchronization of transverse cross sections, a stable pressure distribution, a stationary geometry of the helical shell, an internal force balance, and the existence of stable recirculation zones. The spatial organization of the flow is maintained through the interaction of centrifugal forces, pressure gradients, viscous dissipation, and the continuous input of angular momentum from the rotating disk.

The helical shell may be interpreted as a spatially deformed surface of angular momentum transport localized inside the annular shear layer. At the same time, the structure itself is not an individual concentrated vortex, but rather a modal deformation of the swirling flow within a confined cylindrical volume.

Of particular interest is the relationship between the transverse quadrupole structures and the spatial helical shell. The transverse modes represent horizontal cross sections of a single three-dimensional helical surface, whereas the longitudinal recirculation regions correspond to projections of this spatial structure onto the (r, z) plane. The obtained results show that the helical shell substantially affects the entire hydrodynamic organization of the flow inside the reservoir. The spatial mode induces secondary toroidal recirculation structures, modifies the pressure distribution, and determines the character of admixture transport throughout the fluid volume.

Thus, the considered system demonstrates a transition from an axisymmetric swirling flow to a complex spatially organized modal structure arising from the interaction between rotational motion and an internal stationary obstacle. Moreover, it was observed that the enhancement of admixture concentration near the mean radius of the annular shear layer with increasing azimuthal mode number m is caused by the simultaneous action of three interconnected mechanisms. First, as m increases ($m = 1, 2, 3, 4$), the number of intersections between the deformed vortex shell and the region $r \approx r_s$ increases, thereby raising the probability of particle residence near the mean radius of the layer. Second, a mechanism of parametric dynamical trapping arises, associated with the fact that azimuthal oscillations of the shell create a periodic forcing on the radial motion of particles. When the resonance condition $m\Omega_{shell} \approx \omega_{inertia}$ is satisfied, radial deviations are amplified in such a way that particles remain near r_s for a longer time. Finally, at sufficiently large values of m, when the condition $m > m_{crit}$ is satisfied, the mechanism of diffusive trapping begins to dominate. In this regime, transverse diffusion is no longer able to transport particles beyond the boundaries of the individual azimuthal cells of the shell, and the admixture becomes localized inside the annular layer. All three mechanisms act coherently and lead to an increasingly strong concentration of the admixture within the main annular shear layer as the azimuthal mode number increases.

17. Conclusion.

This work investigates the spatial organization of swirling fluid flow in a cylindrical reservoir with a rotating disk and a stationary central rod. It is shown that the presence of an internal stationary obstacle leads to the formation of an annular shear layer near the rod surface, where strong radial gradients of azimuthal velocity and localized vorticity concentration arise.

Based on spectral decomposition of the perturbation field into azimuthal modes, it is established that the loss of stability of the annular layer is accompanied by the development of non-axisymmetric spatial modes. The results indicate that the most physically consistent mechanism responsible for the observed four-sector structure is the development of the primary dipole mode m=2 followed by nonlinear generation of the second harmonic $m = 4$. As a result, the flow evolves into a mixed modal state $m = 2 + m = 4$, forming a spatial helical shell around the stationary central rod.

It is shown that the quadrupole structure arises as a consequence of nonlinear self-interaction of the dipole mode and redistribution of vorticity within the annular shear layer. The presence of a longitudinal phase shift transforms the transverse azimuthal modes into a unified three-dimensional helical structure extending along the height of the reservoir.

The obtained results demonstrate that the helical shell does not represent an independent concentrated vortex core, but rather a spatially modulated surface of angular momentum transport and vorticity localization surrounding the stationary rod. The stability of this structure is governed by the balance between centrifugal forces, radial pressure gradients, viscous dissipation, and continuous angular momentum input from the rotating disk.

The study further shows that the helical modal structure induces a complex spatial redistribution of velocity, pressure, and vorticity inside the reservoir and leads to the formation of secondary toroidal recirculation zones. The influence region of the helical mode is limited to the domain where the amplitude of azimuthal perturbations remains comparable to the intensity of the primary swirling flow. Outside this region, the flow gradually returns to a quasi-axisymmetric rotational state.

Analysis of passive scalar transport demonstrates that the motion of the tracer is governed by the geometry of the helical channels and secondary recirculation structures, causing the scalar field to stretch into thin spiral concentration filaments that follow the shape of the helical shell.

Thus, the investigated structure may be regarded as a coherent spatial modal organization of the annular swirling layer inside a confined cylindrical volume with an internal stationary obstacle. The proposed physical and mathematical interpretation may be useful for the analysis of swirling flows in vortex devices, rotor reactors, hydrodynamic mixers, intensive liquid mixing systems, and in studies of spatial modes and instabilities in rotating flows.

18. Limitations of the Model.

The physical and mathematical model presented in this work describes the spatial organization of swirling flow in a cylindrical reservoir with a rotating disk and a stationary central rod based on a modal interpretation of the annular shear layer. The proposed approach combines qualitative spectral analysis, modal decomposition, and phenomenological reconstruction of the helical vortex structure. Nevertheless, the model possesses several important limitations associated both with the adopted approximations and with the absence of a complete three-dimensional stability analysis.

Although the present study includes spectral decomposition of the perturbation field into azimuthal Fourier modes and identifies the dominant contributions of the $m = 2$ and $m = 4$ harmonics, a rigorous eigenvalue analysis of the linearized Navier–Stokes operator was not performed. In particular, the complete spectrum of unstable modes, their exact growth rates, and critical transition thresholds were not explicitly calculated. Therefore, the proposed modal selection mechanism should be regarded as a physically motivated spectral model rather than a strict solution of the hydrodynamic stability problem.

In the present work, the quadrupole spatial structure is interpreted primarily as a nonlinear consequence of dipole instability and its second harmonic. However, the relative contributions of centrifugal instability, Kelvin–Helmholtz-type instability, and nonlinear mode interaction were not quantitatively separated. A complete stability analysis would require direct computation of the global eigenmodes of the swirling flow.

Another limitation is associated with the absence of direct numerical simulation of the fully unsteady three-dimensional flow using DNS or LES approaches. The presented helical shells correspond to modal reconstructions and conceptual representations of the annular vortex layer rather than fully resolved turbulent flow fields. Consequently, small-scale turbulent fluctuations and unsteady vortex interactions are not captured within the framework of the present model.

The study also lacks direct experimental validation using PIV measurements, tomographic visualization, laser diagnostics, or other flow measurement techniques. Therefore, the proposed spatial structures should presently be regarded as physically consistent theoretical interpretations of the modal organization of swirling flow.

An additional simplification is associated with the phenomenological representation of the modal amplitude in the form of a Gaussian distribution:

$$A(r,z) = A_0(z)\exp\left[-\left(r - r_0(z)\right)^2/2\sigma_s^2\right],$$

which is introduced to describe the localization region of the helical structure. In reality, the amplitude distribution may depend on boundary conditions, reservoir geometry, angular momentum injection intensity, turbulence level, and nonlinear vortex interactions.

The model also neglects possible effects associated with the free surface, cavitation, unsteady inflow conditions, density stratification, thermal inhomogeneity, and fluid compressibility. The analysis is restricted to the case of an incompressible homogeneous fluid with a statistically stationary mean swirl regime.

Despite these limitations, the proposed interpretation provides a physically consistent description of the mechanism responsible for the loss of axial symmetry in the annular shear layer, the nonlinear interaction of azimuthal modes, and the formation of coherent helical vortex structures around the stationary central rod. The obtained results may serve as a basis for future global stability analysis, fully three-dimensional numerical simulations, and experimental investigations of spatial modes in swirling flows.

References:

1. Batchelor G.K. An Introduction to Fluid Dynamics. Cambridge University Press, 1967.
2. Schlichting H., Gersten K. Boundary Layer Theory. Springer, 2017.
3. Chandrasekhar S. Hydrodynamic and Hydromagnetic Stability. Dover Publications, 1981.
4. Escudier M.P. Observations of the flow produced in a cylindrical container by a rotating endwall. Experiments in Fluids, 1984.
5. Leibovich S. The structure of vortex breakdown. Annual Review of Fluid Mechanics, 1978.
6. Greenspan H.P. The Theory of Rotating Fluids. Cambridge University Press, 1968.
7. Taylor G.I. Stability of a viscous liquid contained between two rotating cylinders. Philosophical Transactions of the Royal Society A, 1923.
8. Gallaire F., Chomaz J.M. Instabilities in swirling flows. Physics of Fluids, 2003.
9. Faler J.H., Leibovich S. Disrupted states of vortex flow and vortex breakdown. Physics of Fluids, 1978.
10. Drazin P.G., Reid W.H. Hydrodynamic Stability. Cambridge University Press, 2004.
11. Vogel H.U. Experimentelle Ergebnisse über die Stabilität der Strömung in einem Spalt zwischen konzentrischen rotierenden Zylindern. Max-Planck-Institut Report, 1968.
12. Lopez J.M., Marques F. Rotating cavity flows and instabilities. Journal of Fluid Mechanics, 2004.
13. Kuibin P.A., Okulov V.L. Helical vortex structures in swirling flows. Thermophysics and Aeromechanics, 1998.
14. Shtern V. Counterflows: Paradoxical Fluid Mechanics Phenomena. Cambridge University Press, 2012.
15. Adrian R.J. Hairpin vortex organization in wall turbulence. Physics of Fluids, 2007.
16. Alekseenko S.V., Kuibin P.A., Okulov V.L. Theory of Concentrated Vortices. Springer, 2007.
17. Panton R.L. Incompressible Flow. Wiley, 2013.
18. Tritton D.J. Physical Fluid Dynamics. Oxford University Press, 1988.
19. Lugt H.J. Vortex Flow in Nature and Technology. Wiley, 1983.
20. Davidson P.A. Turbulence in Rotating, Stratified and Electrically Conducting Fluids. Cambridge University Press, 2013.
21. Milyute E., Milyus A. Mathematical model of flow induced by a rotating disk and kern in a cylindrical reservoir with tangential inlet and radial outlet. In print. 2026.